

Compact3D: Smaller and Faster Gaussian Splatting with Vector Quantization

K L Navaneet*, Kossar Pourahmadi Meibodi*, Soroush Abbasi Koohpayegani,
and Hamed Pirsavash

University of California, Davis

Abstract. 3D Gaussian Splatting (3DGS) is a new method for modeling and rendering 3D radiance fields that achieves much faster learning and rendering time compared to SOTA NeRF methods. However, it comes with the drawback of a much larger storage demand compared to NeRF methods since it needs to store the parameters for millions of 3D Gaussians. We notice that large groups of Gaussians share similar parameters and introduce a simple vector quantization method based on K-means algorithm to quantize the Gaussian parameters. Then, we store the small codebook along with the index of the code for each Gaussian. We compress the indices further by sorting them and using a method similar to run-length encoding. Moreover, we use a simple regularizer that encourages zero opacity (invisible Gaussians) to reduce the number of Gaussians, thereby compressing the model and speeding up the rendering. We do extensive experiments on standard benchmarks as well as an existing 3D dataset that is an order of magnitude larger than the standard benchmarks used in this field. We show that our simple yet effective method can reduce the storage costs for 3DGS by $40\times$ to $50\times$ and rendering time by $2\times$ to $3\times$ with a very small drop in the quality of rendered images. Our code is available here: <https://github.com/UCDvision/compact3d>

1 Introduction

Recently, we have seen great progress in radiance field methods to reconstruct a 3D scene using multiple images captured from multiple viewpoints. NeRF [41] is probably the most well-known method that employs an implicit neural representation to learn the radiance field using a deep model. Although very successful, NeRF methods are very slow to train and render. Several methods have been proposed to solve this problem, however, they usually come with some cost in the quality of the rendered images.

The Gaussian Splatting method (3DGS) [33] is a new paradigm in learning radiance fields. The idea is to model the scene using a set of Gaussians. Each Gaussian has several parameters including its position in 3D space, covariance matrix, opacity, color, and spherical harmonics of the color that need to be learned from multiple-view images. Thanks to the simplicity of projecting 3D

* Equal contribution

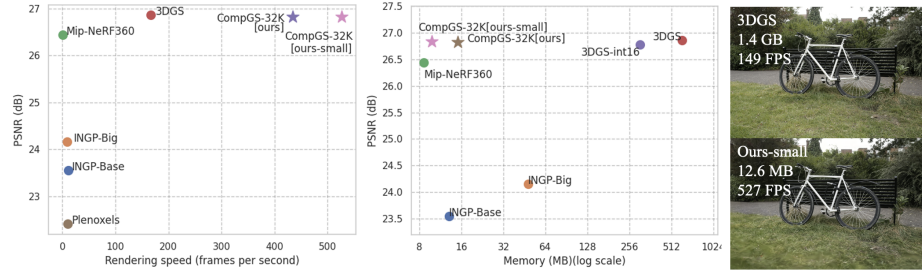


Fig. 1: Comparison of performance, inference speed, and memory time. CompGS, our compressed version of 3DGS, maintains the speed and performance of 3DGS while reducing its size to the levels of NeRF based approaches. We achieve around 45× compression and 2.5× inference speed up with little drop in performance (CompGS-32K). A highly regularized variant, CompGS-32K-small trades-off performance for even higher compression of 90× on an average.

Gaussians to the 2D image space and rasterizing them, 3DGS is significantly faster to both train and render compared to NeRF methods. This results in real-time rendering of the scenes on a single GPU (ref. Fig. 1). Additionally, unlike the implicit representations in NeRF, the 3D structure of the scene is explicitly stored in the parameter space of the Gaussians. This enables many operations including editing the 3D scene directly in the parameter space.

One of the main drawbacks of the 3DGS method compared to NeRF variants is that 3DGS needs at least an order of magnitude more parameters compared to NeRF. This increases the storage and communication requirements of the model and its memory at the inference time, which can be very limiting in many real-world applications involving smaller devices. For instance, the large memory consumption may be prohibitive in storing, communicating, and rendering several radiance field models on AR/VR headsets.

We are interested in compacting 3DGS representations without sacrificing their rendering speed to enable their usage in various applications including low-storage or low-memory devices and AR/VR headsets. Our main intuition is that several Gaussians may share some of their parameters (e.g. covariance matrix). Hence, we simply vector-quantize parameters and store the codebook along with the index for each Gaussian. This can result in a huge reduction in the storage. Also, it can reduce the memory footprint at the rendering time since the index can act as a pointer to the correct code freeing the memory needed to replicate those parameters for all Gaussians.

To this end, we use simple K-means algorithm to vector quantize the parameters at the learning time. Inspired by various quantization-aware learning methods in deep learning [49], we use the quantized model in the forward pass while updating the non-quantized model in the backward pass. To reduce the computation overhead of running K-means, we update the centroids in each iteration, but update the assignments less frequently (e.g., once every 100 iterations) since it is costly. Moreover, since the Gaussians are a set of non-ordered elements, we compress the representation further by sorting the Gaussians based on one of

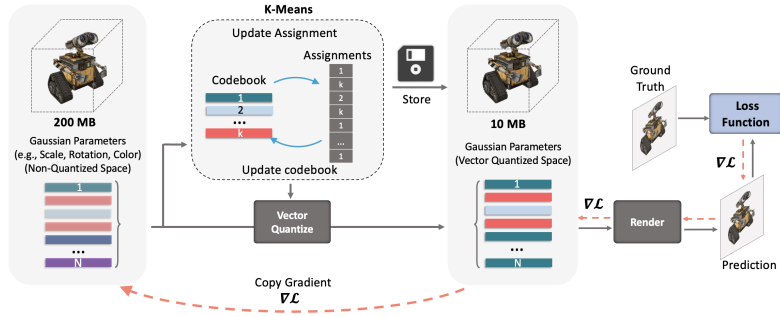


Fig. 2: Overview of CompGS vector quantization: We compress 3DGS using vector quantization of the parameters of the Gaussians. The quantization is performed along with the training of the Gaussian parameters. Considering each Gaussian as a vector, we perform K-means clustering to represent the N Gaussians in the model with k cluster centers (codes). Each Gaussian is then replaced by its corresponding code for rendering and loss calculation. The gradients wrt centers are copied to all the elements in the corresponding cluster and the non-quantized versions of the parameters are updated. Only the codebook and code assignments for each Gaussian are stored and used for inference. CompGS maintains the real-time rendering property of 3DGS while compressing it by an order of magnitude.

the quantized indices and storing them using the Run-Length-Encoding (RLE) method. Furthermore, we employ a simple regularizer to promote zero opacity (essentially invisible Gaussians), resulting in significant reductions in storage and rendering time by reducing the number of Gaussians. Our final model is $40\times$ to $50\times$ smaller and $2\times$ to $3\times$ faster during rendering compared to 3DGS.

Unlike visual recognition community that uses large scale benchmarks, interestingly, radiance field modeling community traditionally has used small datasets with a handful of 3D scenes: maximum of 13 total real world scenes in several papers (e.g., 3DGS [33]). We believe this is due to the computational cost of NeRF-based methods (several hours of training time for each scene). Hence, with the recent advancements in this field including 3DGS that takes only a few minutes to learn a scene, it may be time to move beyond small benchmarks and evaluate methods on larger scale benchmarks. Therefore, we use an existing scene-understanding dataset [6] as a benchmark for radiance field modeling that is an order of magnitude larger than the traditional datasets (200 vs 13 scenes). We believe the community will benefit from using this larger benchmark to evaluate future radiance field methods with a reasonable computational demand. Note that we are not claiming any novelty in this dataset as it is not collected by us.

2 Related Work

Novel-view synthesis methods: Early deep learning techniques for novel-view synthesis used CNNs to estimate blending weights or texture-space solu-

tions [17, 27, 53, 59, 67]. However, the use of CNNs faced challenges with MVS-based geometry and caused temporal flickering. Volumetric representations began with Soft3D [47], and subsequent techniques used deep learning with volumetric ray-marching [29, 55]. Mildenhall et al. introduced Neural Radiance Fields (NeRFs) [41] to improve the quality of synthesized novel views, but the use of a large Multi-Layer Perceptron (MLP) as the backbone and dense sampling slowed down the process a lot. Successive methods sought to balance quality and speed, with Mip-NeRF360 achieving top image quality [4]. Recent advances prioritize faster training and rendering via spatial data structures, encodings, and MLP adjustments [10, 18, 19, 28, 43, 52, 57, 64, 66]. Notable methods, like InstantNGP [43], use hash grids and occupancy grids for accelerated computation with a smaller MLP, while Plenoxels [18] entirely forgo neural networks, relying on Spherical Harmonics for directional effects. Despite impressive results, challenges in representing empty space, limitations in image quality, and rendering speed persist in NeRF methods. In contrast, 3DGS [33] achieves superior quality and faster rendering without implicit learning [4]. However, the main drawback of 3DGS is its increased storage compared to NeRF methods which may limit its usage in many applications such as edge devices. We are able to keep the quality and fast rendering speed of 3DGS method while providing reduced model storage by applying a vector quantization scheme to Gaussian parameters.

Bit Quantization: Reducing the number of bits to represent each parameter in a deep neural network is a commonly used method to quantize models [26, 32, 35] that result in smaller memory footprints. Representing weights in 64 or 32-bit formats may not be crucial for a given task, and a lower-precision quantization can lead to memory and speed improvements. Dettmers et al. [14] show 8-bit quantization is sufficient for large language models. In the extreme case, weights of neural networks can be quantized using binary values. XNOR [50] examines this extreme case by quantization-aware training of a full-precision network that is robust to quantization transformations.

Vector Quantization: Vector quantization (VQ) [15, 20, 22, 23] is a lossy compression technique that converts a large set of vectors into a smaller codebook and represents each vector by one of the codes in the codebook. As a result, one needs to store only the code assignments and the codebook instead of storing all vectors. This compression technique has been used in many applications including image compression [12], video and audio codec [37, 40], compressing deep networks [11, 22], and generative models [24, 51, 60]. We apply a similar method to compressing 3DGS models.

Compression for 3D scene representation methods. Since NeRF relies on dense sampling of color values and opacity, the computational costs are significant. To efficiently represent 3D scenes and objects, methods adopt different data structures such as trees [62, 66], point clouds [46, 65], and grids [8, 18, 43, 54, 56, 57]. With grid structures training iterations can be completed in a matter of minutes. However, dense 3D grid structures may require substantial amounts of memory. Several methods have worked on reducing the size of such volumet-

ric grids [8, 43, 57, 58]. Instant-NGP [43] uses hash-based multi-resolution grids. VQAD [57] replaces the hash function with codebooks and vector quantization.

Another line of work decomposes 3D grids into lower dimensional components, such as planes and vectors, to reduce the memory requirements [8, 31, 58]. Despite reducing the time and space complexity of the 3D scenes, their sizes are still larger than MLP-based methods. VQRF [38] compresses volumetric grid-based radiance fields by adopting the VQ strategy to encode color features into a compact codebook.

While we also employ vector quantization, we differ from the above approaches in the method employed for novel view synthesis. Unlike the NeRF based approaches described above, we aim to compress 3DGS which uses a collection of 3D Gaussians to represent the 3D scene and does not contain grid like structures or neural networks. We also achieve a significant amount of compression by regularizing and pruning the Gaussians based on their opacity. Some very recent works [16, 21, 36, 42, 44] also propose methods to compress 3D Gaussian splat models. Note that these works are concurrent to ours.

Deep Model Compression. Model compression tries to reduce the storage size without changing the accuracy of original models. Model compression techniques can be divided to 1) model pruning [25, 26, 61, 63] that aims to remove redundant layers of neural networks; 2) weight quantization [32, 35, 45], and 3) knowledge distillation [2, 3, 9, 30, 48], in which a compact student model is trained to mimic the original teacher model. Some works have applied these techniques to volumetric radiance fields [13, 39, 66]. For instance, TensoRF [8] decompose volumetric representations via low-rank approximation.

3 Method

Here, we briefly describe the 3DGS [33] method for learning and rendering 3D scenes and explain our vector quantization approach for compressing it.

Overview of 3DGS: 3DGS models a scene using a collection of 3D Gaussians. A 3D Gaussian is parameterized by its position and covariance matrices in the 3D space. $G(x) = e^{-\frac{1}{2}(x-\mu)^T \Sigma^{-1}(x-\mu)}$ where $x - \mu$ is the position vector, μ is the position, and Σ is the 3D covariance matrix of the Gaussian. Since the covariance matrix needs to be positive definite, it is factored into its scale (S) and rotation (R) matrices as $\Sigma = RSS^T R^T$ for easier optimization. In addition, each Gaussian has an opacity parameter σ . Since the color of the Gaussians may depend on the viewing angle, the color of each Gaussian is modeled by a Spherical Harmonics (SH) of order 3 in addition to a DC component.

Given a view-point, the collection of 3D Gaussians is efficiently rendered in a differentiable manner to get a 2D image by α -blending of anisotropic splats, sorting, and using a tile-based rasterizer. Color of a pixel is given by $C = \sum_i c_i \alpha_i \prod_{j=1}^{i-1} (1 - \alpha_j)$ where c_i is the color of the i^{th} Gaussian and α_i is the product of the value of the Gaussian at that point and its learned opacity σ_i . At the training time, 3DGS renders the training view points and minimizes the loss between the groundtruth and rendered images in the pixel space. The loss

is ℓ_1 loss plus an SSIM loss in the pixel space. 3DGS initializes the optimization by a point cloud achieved by a standard SfM method and iteratively prunes the ones with small opacity parameter and adds new ones when the gradient is large. 3DGS paper shows that it is extremely fast to train and is capable of real-time rendering while matching or outperforming SOTA NeRF approaches in terms of 3D model quality.

Compression of 3DGS:

We compress the parameters of 3DGS using vector quantization aware training and reduce the number of Gaussians in the model by regularizing the opacity parameter.

Vector quantization: 3DGS requires a few million Gaussians to model a typical scene. With 59 parameters per Gaussian, the storage size of the trained model is an order of magnitude larger than most NeRF approaches (e.g., Mip-NeRF360 [4]). This makes it inefficient for some applications including edge devices. We are interested in reducing the number of parameters. Our main intuition is that many Gaussians may have similar parameter values (e.g., covariance). Hence, we use simple vector quantization using K-means algorithm to compress the parameters. Fig. 2 provides an overview of our approach.

Consider a 3DGS model with N Gaussians, each with a d dimensional parameter vector. We run K-means algorithm to cluster the vectors into K clusters. Then, one can store the model using K vectors of size d and N integer indices (one for each Gaussian). Since $N \gg K$, this method can result in a large compression ratios. In a typical scene, N is a few millions while K is a few thousands.

However, just clustering the trained model parameters results in performance degradation. We need to perform quantization aware training to ensure that the model parameters are amenable to quantization. In learning the parameters of 3DGS model, we store the non-quantized parameters. In the forward pass of learning 3DGS, we quantize the parameters and replace them with the quantized version (centroids) to do the rendering and calculate the loss. Then, we do the backward pass to get the gradients for the quantized parameters and copy the gradients to the non-quantized parameters to update them. We use straight-through estimator proposed in STE [7]. After learning, we discard the non-quantized parameters and keep only the codebook and indices of the codes for Gaussians.

Since the number of Gaussians N is typically in millions, cost of performing K-means at every iteration of training can be prohibitively high. K-means has two steps: updating centroids given assignments, and updating assignments given centroids. We note that the latter is more expensive while the former is a simple averaging. Hence, we update the centroids after each iteration and update the assignments once every t iterations. We observe that the modified approach works well even for values of t as high as 500. This is crucial in limiting the training time of the method.

Performing a single K-means for the whole d dimensional parameters requires a huge codebook since the different parameters of the Gaussian are not necessarily correlated. Hence, we group similar parameters together and cluster them

independently to learn a separate codebook for each. This requires storing multiple indices for each Gaussian. In our main method, we quantize DC component of color, spherical harmonics, scale, and rotation parameters separately, resulting in 4 codebooks. We do not quantize opacity parameter since it is a single scalar and do not quantize the position of the Gaussians since sharing them results in overlapping Gaussians which does not make sense.

Since the indices are integer values, we use fewer number of bits compared to the original parameters to store each. Moreover, 3DGS models the scene as a set of Gaussians where the ordering does not matter. Hence, we sort the Gaussians based on one of the indices so that Gaussians using the same code appear together in the list. Then, for that index, instead of storing n integers, we store the index of the Gaussian that the index of its code in the codebook increases by one. This is similar to run-length-coding for data compression. This method reduces the size of one of the indices from n integers to k integers.

Opacity Regularization: Some parameters like position of the Gaussians cannot be quantized easily, so as shown in Table 5 after quantization, the memory is dominated (more than 80% of memory) by such parameters. This means quantization cannot improve the compression any further. One way to compress 3DGS more is to reduce the number of Gaussians. Interestingly, this reduction comes with a bi-product that is increase in inference time. This can be an important improvement in many applications (particularly when the rendering is happening in small devices.)

We know that very small values of opacity (σ) correspond to transparent or nearly invisible Gaussians. Hence, inspired by training sparse models, we add a new loss term to encourage zero values for opacity. We do so by simply using the ℓ_1 of the opacity values as a regularizer. Hence the final loss becomes: $\mathcal{L} = \mathcal{L}_{3DGS} + \lambda_{reg} \sum_i^N \sigma_i$, where \mathcal{L}_{3DGS} is the original loss of 3DGS with or without quantization and λ_{reg} controls the sparsity of opacity. Finally, similar to the original 3DGS, we remove the Gaussians with opacity smaller than a threshold. This results in significant reduction in storage and inference time.

4 Experiments

4.1 Implementation Details

For all our experiments, we use the publicly available official code repository [1] of 3DGS [33] provided by its authors. There are no changes in the hyperparameters used for training compared to 3DGS. The Gaussian parameters are trained without any vector quantization till $20K$ iterations and K-means quantization is used for the remaining $10K$ iterations. A standard K-means iteration involves distance calculation between all elements (Gaussian parameters) and all cluster centers followed by assignment to the closest center. The centers are then updated using new cluster assignments and the loop is repeated. We use just 1 such K-means iteration in our experiments once every 100 iterations till iteration $25K$ and keep the assignments constant thereafter till the last iteration, $30K$. The K-means cluster centers are updated using the non-quantized

Table 1: Comparison with SOTA methods for novel view synthesis. 3DGS [33] performs comparably or outperforms the best of the NeRF based approaches while maintaining a high rendering speed during inference. Trained NeRF models are significantly smaller than 3DGS since NeRFs are parameterized using neural networks while 3DGS requires storage of parameters of millions of 3D Gaussians. CompGS is a vector quantized version of 3DGS that maintains the speed and performance advantages of 3DGS while being **40× to 50× smaller**. *Reproduced using official code. [†] Reported from 3DGS [33]. Our timings for 3DGS and CompGS are reported using a RTX6000 GPU while those with [†] used A6000 GPU. We boldface entries for emphasis.

Method	Mip-NeRF360						Tanks&Temples						Deep Blending					
	SSIM [†]	PSNR [†]	LPIPS [†]	FPS	Mem (MB)	Train Time(m)	SSIM [†]	PSNR [†]	LPIPS [†]	FPS	Mem (MB)	Train Time(m)	SSIM [†]	PSNR [†]	LPIPS [†]	FPS	Mem (MB)	Train Time(m)
Plenoxels [†]	0.626	23.08	0.463	6.79	2100	25.5	0.719	21.08	0.379	13.0	2300	25.5	0.795	23.06	0.510	11.2	2700	27.5
INGP-Base [†]	0.671	25.30	0.371	11.7	13	5.37	0.723	21.72	0.330	17.1	13	5.26	0.797	23.62	0.423	3.26	13	6.31
INGP-Big [†]	0.691	25.59	0.331	9.43	48	7.30	0.745	21.92	0.305	14.4	48	6.59	0.817	24.96	0.390	2.79	48	8.00
M-NeRF360 [†]	0.792	27.69	0.237	0.06	8.6	48h	0.759	22.22	0.257	0.14	8.6	48h	0.901	29.40	0.245	0.09	8.6	48h
3DGS [†]	0.815	27.21	0.214	134	734	41.3	0.841	23.14	0.183	154	411	26.5	0.903	29.41	0.243	137	676	36.2
3DGS *	0.813	27.42	0.217	149	778	21.6	0.844	23.68	0.178	206	433	12.2	0.899	29.49	0.246	151	662	19.3
CompGS 16K	0.804	27.03	0.243	346	18	22.8	0.836	23.39	0.200	479	12	15.6	0.906	29.90	0.252	485	12	20.3
CompGS 32K	0.806	27.12	0.240	344	19	29.4	0.838	23.44	0.198	475	13	20.6	0.907	29.90	0.251	484	13	26.2

Gaussian parameters after each iteration of training. The covariance (scale and rotation) and color (DC and harmonics) components of each Gaussian is vector quantized while position (mean) and opacity parameters are not quantized. Additional results with different parameters being quantized are provided in Table 8. Unless mentioned differently, we use a codebook of size 4096 for the color and 16384 (CompGS 16K) for the covariance parameters. The scale parameters of covariance are quantized before applying the exponential activation on them. Similarly, quaternion based rotation parameters are quantized before normalization. For opacity regularization, we use $\lambda_{\text{reg}} = 10^{-7}$ from iterations 15K to 20K along with opacity based pruning every 1000 iterations and remove regularization thereafter. All experiments were run on a single RTX-6000 GPU.

Datasets: We primarily show results on three challenging real world datasets - Tanks&Temples [34], Deep Blending [27] and Mip-NeRF360 [4] containing two, two and nine scenes respectively. Additionally, we provide results on a subset of the large scale ARKit [6] dataset. Our ARKit subset is an order of magnitude larger than the other datasets with 200 scenes. ARKit [6] is an indoor scene understanding dataset comprising 5,048 scans encompassing 1,661 distinct scenes. The videos are recorded using the 2020 iPad Pro and have a resolution of 1920×1440 . We exclusively utilize the RGB frames from each video. To construct the dataset subset for view synthesis, we randomly select 200 raw videos from the ARKit dataset, extracting a uniform sample of 300 frames from each. Subsequently, we employ the code provided by 3DGS [33] to extract undistorted images and Structure-from-Motion (SfM) information from the input images. The dataset can easily be extended in the future by including more of the remaining scenes from the ARKit dataset.

Baselines: As we propose a method (termed CompGS) for compacting 3DGS, we focus our comparisons with 3DGS and different baseline methods for compressing it. We consider bit quantization (denoted as Int-16/8/4 in results) and 3DGS without the harmonic components for color (denoted as 3DGS-No-SH) as alternative parameter compression methods. Bit-quantization is performed using the standard Absmax quantization [14] technique. Similarly, we consider several alternative approaches to reduce the number of Gaussians. Densification process in 3DGS increases the Gaussian count and is controlled by the gradient threshold (termed grad thresh) parameter and the frequency (freq) and iterations (iters) until densification is performed. The opacity threshold (min opacity) controls the pruning of transparent Gaussians. We modify these parameters in 3DGS to compress the model with as little drop in performance as possible. Additionally, Table 1 shows comparison with state-of-the-art NeRF approaches [4, 18, 43]. Mip-NeRF360 [4] achieves high performance comparable to 3DGS while Plenoxtels [18] and InstantNGP [43] have high frame-rate for rendering and very low training time. InstantNGP and Mip-NeRF360 are also comparable in model size to our compressed model.

Evaluation: For a fair comparison, we use the same train-test split as Mip-NeRF360 [4] and 3DGS [33] and directly report the metrics for other methods from 3DGS [33]. We also report our reproduced metrics for 3DGS since we observe slightly better results compared to the ones in [33]. We report the standard evaluation metrics of SSIM, PSNR and LPIPS along with memory or compression ratio, rendering FPS and training time. The common practice is to report the average of PSNR across a set of images and scenes. However, this metric may be dominated by very accurate reconstructions (smaller errors) since it is based on the geometric average of the errors due to the log operation in PSNR calculation. Hence, for the larger ARKit dataset, we also report PSNR-AM for which we average the error across all images and scenes before calculating the PSNR. In comparing model sizes, we normalize all methods by dividing them by the size of our method to obtain compression ratio.

4.2 Main Results

Comparison of our results with state-of-the-art (SOTA) novel view synthesis approaches is shown in Table 1. Our vector quantized method has a comparable performance to the non-quantized 3DGS with a small drop on MipNerf-360 and TandT datasets and a small improvement on the DB dataset. The model memory footprint drastically reduces for CompGS compared to 3DGS, making it comparable to NeRF approaches. **Our models are 41×, 33× and 51× smaller** than 3DGS models on MipNerf-360, TandT and DB datasets respectively. This reduces a big disadvantage of 3DGS models and makes them more practical. The compression achieved by CompGS is impressive considering that more than two-thirds of its memory is due to the non-quantized position and opacity parameters (refer table 5). Additionally CompGS maintains the other advantages of 3DGS such as low inference memory usage and training time. while also **increasing its**

Table 2: Comparison of parameter compression methods for 3DGS. We evaluate different baseline approaches for compressing the parameters of 3DGS without any reduction in the number of Gaussians. All memory values are reported as a ratio of the method with our smallest model. Our K-Means based vector quantization performs favorably compared to all methods both in terms of novel view synthesis performance and compression. Not quantizing the position values (Int-x no-pos) is crucial in bit quantization. Since harmonics constitute 76% of each Gaussian, 3DGS-no-SH achieves a high level of compression. But CompGS with only quantized harmonics achieves similar compression with nearly no loss in performance compared to 3DGS .

Method	Mip-NeRF360			Tanks&Temples			Deep Blending			Mem
	SSIM	PSNR	LPIPS	SSIM	PSNR	LPIPS	SSIM	PSNR	LPIPS	
3DGS	0.813	27.42	0.217	0.844	23.68	0.178	0.899	29.49	0.246	20.0
3DGS-No-SH	0.802	26.80	0.229	0.833	23.16	0.190	0.900	29.50	0.247	4.8
Post-train K-means 4K	0.768	25.46	0.266	0.803	22.12	0.226	0.887	28.61	0.268	1.7
K-means 4K Only-SH	0.811	27.25	0.223	0.842	23.57	0.183	0.902	29.60	0.246	4.8
K-means 4K	0.804	26.97	0.234	0.836	23.31	0.194	0.904	29.76	0.248	1.7
K-means 32K	0.808	27.16	0.228	0.840	23.47	0.188	0.903	29.75	0.247	1.8
Int16	0.804	27.25	0.223	0.836	23.56	0.185	0.900	29.49	0.247	10.0
Int8 no-pos	0.812	27.38	0.219	0.843	23.67	0.180	0.900	29.47	0.247	5.8
Int8	0.357	14.41	0.629	0.386	12.37	0.625	0.709	21.58	0.457	5.0
Int4 no-pos	0.489	17.42	0.525	0.488	12.94	0.575	0.746	19.90	0.446	3.4
3DGS-No-SH Int16	0.789	26.59	0.237	0.826	23.04	0.198	0.900	29.50	0.248	2.4
K-means 4K, Int16	0.796	26.83	0.239	0.830	23.21	0.199	0.904	29.76	0.248	1.0

already impressive rendering FPS by 2 \times to 3 \times . A limitation of CompGS compared to 3DGS is the overhead in compute and training time introduced by the K-means clustering algorithm. This is compensated in part by the reduced compute and time due to the decrease in Gaussian count. CompGS 16K variant requires marginally more time than 3DGS while CompGS 32K needs 1.4 \times to 1.7 \times more training time. However, this is still orders of magnitude smaller than the high-quality NeRF based approaches like MipNerf-360. Per-scene evaluation metrics are in supplementary.

We decouple our compression method into parameter and Gaussian count compression components and perform ablations on each of them.

Comparison of parameter compression methods: In Table 2, we compare the proposed vector quantization based compression against other baseline approaches for compressing 3DGS. Since the spherical harmonic components used for modeling color make up nearly three-fourths of all the parameters of each Gaussian, a trivial compression baseline is to use a variant of 3DGS with only the DC component for color and no harmonics. This baseline (3DGS-No-SH) achieves a high compression with just 23.7% of the original model size but has a drop in performance. Our K-Means approach outperforms 3DGS-No-SH while using less than half its memory. We also consider a variant of CompGS with a single codebook for both SH and DC parameters (termed SH+DC) with a larger codebook of size of 4096. This has a marginal decrease in both memory and per-

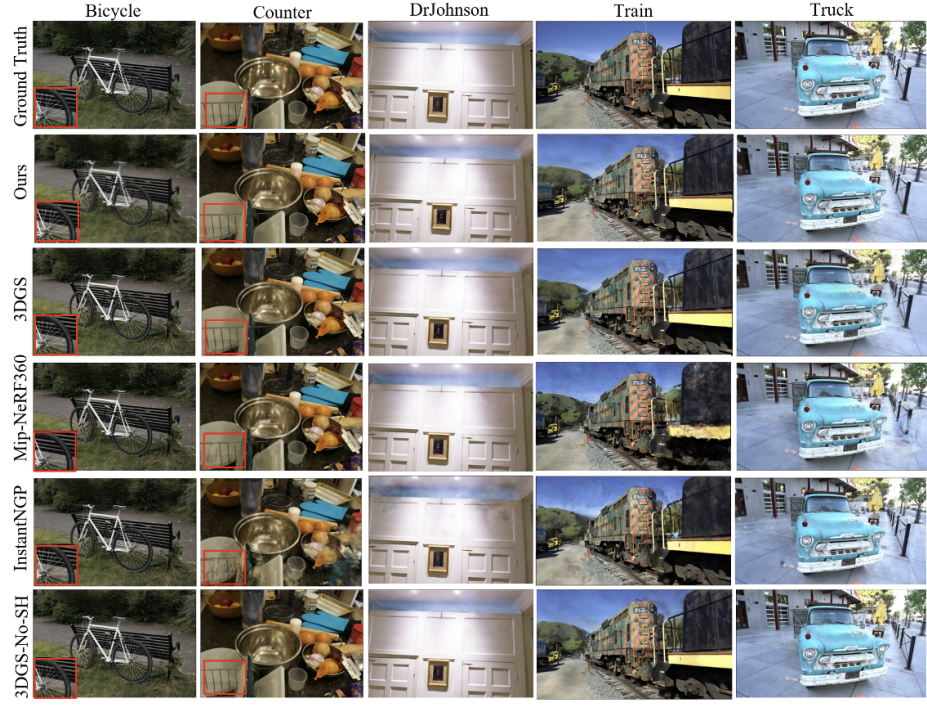


Fig. 3: Qualitative comparison of novel view synthesis approaches. We visualize images from different scenes across datasets for SOTA Nerf, 3DGS, our CompGS and the No-SH variant of 3DGS. All methods based on 3DGS have better reconstruction of finer details like spokes of the bicycle wheel compared to NeRF approaches. Both compressed versions CompGS and 3DGS-No-SH are similar in appearance to 3DGS with no additional visually apparent errors.

formance compared to default CompGS suggesting that correlated parameters can be combined to reduce the number of indices to be stored.

Fig. 3 shows qualitative comparison of CompGS across multiple datasets with both SOTA approaches and compression methods for 3DGS. Both CompGS and 3DGS-No-SH are visually similar to 3DGS, preserving finer details such as the spokes of the bike and bars of dish-rack. Among NeRF approaches, Mip-NeRF360 is closest in terms of quality to 3DGS while InstantNGP trades-off quality for inference and training speed.

All the above approaches are trained using 32-bit precision for all Gaussian parameters. Post-training bit quantization of 3DGS to 16-bits reduces the memory by half with very little drop in performance. However, reducing the precision to 8-bits results in a huge degradation of the model. This drop is due to the quantization of the position parameters of the Gaussians. Excluding them from quantization (denoted as Int8 no-pos) results in a model comparable to the 32-bit variant. However, further reduction to 4-bits degrades the model even when the position parameters are not quantized. Note that bit quantization approaches

Table 3: Reducing number of Gaussians in 3DGS. We evaluate different baseline approaches for compressing 3DGS by reducing the number of Gaussians. Gaussian count is proportional to model size. CompGS performs favorably compared to all methods both in terms of novel view synthesis performance and compression. Entries boldfaced for emphasis.

Method	Mip-NeRF360						Tanks&Temples						Deep Blending					
	SSIM	PSNR	LPIPS	#Gauss	SSIM	PSNR	LPIPS	#Gauss	SSIM	PSNR	LPIPS	#Gauss	SSIM	PSNR	LPIPS	#Gauss		
3DGS	0.813	27.42	0.217	3.30M	0.844	23.68	0.178	1.83M	0.899	29.49	0.246	2.80M						
Min Opacity	0.802	27.12	0.244	1.46M	0.833	23.44	0.204	780K	0.902	29.50	0.255	1.01M						
Densify Freq	0.794	26.98	0.255	1.07M	0.832	23.36	0.206	709K	0.902	29.76	0.258	844K						
Densify Iters	0.780	27.02	0.267	1.12M	0.835	23.55	0.194	810K	0.896	29.42	0.264	795K						
Grad Thresh	0.769	26.57	0.292	809K	0.825	23.31	0.217	578K	0.900	29.49	0.260	1.01M						
Opacity Reg	0.813	27.42	0.227	845K	0.844	23.71	0.188	520K	0.905	29.73	0.249	554K						

Table 4: Comparison of results on the large scale ARKit dataset. The benchmark contains 200 scenes from the ARKit [5] indoor scene understanding dataset. We report results for just the vector quantized version of CompGS . (left) CompGS achieves a high level of compression with nearly identical metrics for view synthesis. Compressing such large scale indoor scenes can be particularly helpful for VR applications. (right) 3DGS-No-SH fails to reconstruct well in several images while CompGS is nearly identical to 3DGS with a large reduction in model size.

Method	Ground Truth					CompGS [ours]					3DGS					3DGS-No-SH				
	SSIM	PSNR	PSNR-AM	LPIPS	Mem	SSIM	PSNR	PSNR-AM	LPIPS	Mem	SSIM	PSNR	PSNR-AM	LPIPS	Mem	SSIM	PSNR	PSNR-AM	LPIPS	Mem
3DGS	0.909	25.76	20.73	0.226	20.0															
3DGS-No-SH	0.905	25.31	20.11	0.234	4.8															
CompGS	0.909	25.70	20.73	0.229	1.7															



offer significantly lower compression compared to CompGS and they are a subset of the possible solutions for our vector quantization method. Similar to 3DGS, CompGS has a small drop in performance when 16-bit quantization is used.

Comparison of Gaussian count compression methods: In Table 3, we compare the proposed opacity regularization method for reducing the Gaussian count with baselines. In these baselines, we modify the 3DGS parameters to decrease densification and increase pruning and thus reduce the number of Gaussians. We report the best metrics for each baseline here (refer suppl. for ablation). Our opacity regularization results in $3.5\times$ to $5\times$ reduction in Gaussian count with nearly identical performance as the larger models. Similar level of compression is achieved only by the gradient threshold baseline that reduces densification. However, it results in a large drop in performance.

Results on ARKit dataset: Table 4 shows the quantitative and qualitative results on our large-scale ARKit benchmark. Our compressed model achieves nearly the same performance as 3DGS with ten times smaller memory. Unlike CompGS , the 3DGS-No-SH method suffers a significant drop in quality. We also

report PSNR-AM as the PSNR calculated using arithmetic mean of MSE over all the scenes in the dataset to prevent the domination of high-PSNR scenes.

4.3 Ablations

We analyze our design choices and the effect of various hyperparameters on reconstruction performance and model size.

Memory break-down of CompGS: In Table 5, we show the contribution of various components to the final memory usage of CompGS. Out of 59 parameters of each Gaussian, we quantize 55 parameters of color and covariance while the 3 position and 1 opacity parameters are used as is. However, the bulk of the stored memory (68% and 81% for 16- and 32-bits) is due to the non-quantized parameters. For the quantized parameters, nearly all the memory is used to store the cluster assignment indices with less than 2% used for the codebook.

Trade-off between performance, compression and training time: Compressing the Gaussian parameters comes with a trade-off, particularly between performance and training time. In our vector quantization, the size of codebook, frequency of code assignment and number of iterations in code computation control this trade-off. Similarly, regularization strength can be modified in Gaussian count reduction to obtain a trade-off between performance and compression. We show ablations on these hyperparameters in tables 6 and 7. CompGS offers great flexibility, with different levels of compression and training time without sacrificing much on performance.

Parameter selection for quantization: Table 8 shows the effect of quantizing different subsets of the Gaussian parameters on the Tanks&Temples dataset. Quantizing the position parameters significantly reduces the performance on both the scenes. We thus do not quantize position in any of our other experiments. Quantizing only the harmonics (SH) of color parameter is nearly identical in size to the no-harmonics (3DGS-No-SH) of 3DGS. Our SH has very little

Table 5: Breakdown of memory usage in CompGS. We observe that just 4 non-quantized values of the total 59 values per Gaussian contribute to 68% and 81% of the total memory in our 16-bit and 32-bit variants respectively. For the quantized parameters, nearly the entire memory is used to store the indices.

	Non Quant	Quant	k-Means	Quantization
	Quant	Quant	Index	Codebook
Num Params	4	55		
Mem (16bit)	68%	32%	99%	1%
Mem (32bit)	81%	19%	98%	2%

Table 6: Compression-performance tradeoff. Gaussian count decreases drastically with heavy regularization but also results in some drop in performance on Mip-NeRF360 dataset. We choose $\lambda = 10^{-7}$ as default.

$\lambda_{\text{reg}} (\times 10^{-7})$	SSIM	PSNR	LPIPS	#Gauss
0.5	0.808	27.17	0.234	1.21M
1.0	0.806	27.12	0.240	845K
2.0	0.801	26.98	0.253	536K
3.0	0.794	26.83	0.266	390K

Table 7: Performance and training time trade-off. Depending on user’s needs, it is possible to obtain models with fast training or high performance. The hyperparameters of vector quantization - number of K-Means iterations (iters), K-Means frequency (freq) and codebook size (#codes) can be varied to obtain the desired point on the curve. They offer a good trade-off, with huge decrease in training time with minor changes in performance. Results are shown on MipNerf-360.

Iters	Freq	#Codes	SSIM	PSNR	Time
1	100	8K	0.802	26.94	19.3
3	100	8K	0.802	26.94	20.9
5	100	8K	0.802	26.95	22.5
10	100	8K	0.802	26.95	26.5
5	50	8K	0.803	27.00	28.7
5	200	8K	0.799	26.76	19.4
5	500	8K	0.783	26.15	18.1
5	100	4K	0.800	26.84	19.6
5	100	16K	0.804	27.05	28.9
5	100	32K	0.806	27.12	42.4

Table 8: Effect of quantization on different Gaussian parameters. Each Gaussian in 3DGS is parameterized using position (pos), scale, rotation (rot) and color (DC and harmonics SH). We analyze the effect of quantizing combinations of these parameters on the view synthesis performance. SH+DC denotes that a single codebook is used for both SH and DC. Position values cannot be quantized without greatly affecting model performance. The rest of the parameters can be simultaneously combined to obtain a high degree of compression without much loss in quality.

Quantized Params	Train		Truck		Mem
	SSIM [†]	PSNR [†]	SSIM [†]	PSNR [†]	
3DGS	0.811	21.99	0.878	25.38	20.0
3DGS-No-SH	0.798	21.40	0.871	24.92	4.8
Variants of CompGS					
Pos	0.673	19.81	0.730	21.65	19.0
SH	0.809	21.88	0.876	25.27	4.8
SH, DC	0.806	21.68	0.875	25.24	3.8
Rot(R)	0.808	21.83	0.876	25.32	18.7
Scale(Sc)	0.809	21.79	0.877	25.30	19.0
SH,R	0.805	21.67	0.874	25.20	3.5
SH,Sc	0.806	21.63	0.875	25.18	3.8
SH,Sc,R	0.801	21.64	0.872	25.02	2.6
SH+DC,Sc,R	0.797	21.41	0.868	24.89	1.6
SH,DC,Sc,R	0.801	21.64	0.871	24.97	1.7
SH,DC,Sc,R Int16	0.790	21.49	0.869	24.93	1.0

drop in metrics compared to 3DGS while 3DGS-No-SH is much worse off without the harmonics. As more parameters are quantized, the performance of CompGS slowly reduces. The combination of all color and covariance parameters still results in a model with good qualitative and quantitative results.

Effect of codebook size: Fig. 4 shows the effect of codebook length on reconstruction performance for quantization of different Gaussian parameters on the Tanks&Temples dataset. The DC component of color has the smallest drop in performance upon quantization and achieves results similar to the non-quantized version with as few as 128 cluster centers. The harmonics (SH) components of color lead to a much bigger drop at lower number of clusters and improve as more clusters are added. Note that CompGS with only SH components is nearly the same size as 3DGS-No-SH but has a much better performance (23.43 for ours v/s 23.14 for 3DGS-No-SH). The covariance parameters (rotation and scale) have a drop in performance even at a codebook size of 1024 but improve as the codebook size is increased.

Generalization of codebook across scenes We train our vector quantization approach including the codebook and the code assignments on a single scene

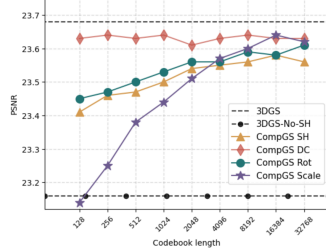


Fig. 4: Effect of codebook length. We vary codebook length independently for the four (SH, DC, Rotation, Scale) parameters by quantizing just one of them.

(‘Counter’) of the Mip-NeRF360 dataset. We then freeze the codebook and learn only assignments for the rest of the eight scenes in the dataset and report the averaged performance metrics over all scenes (Fig. B.2). Interestingly, we observe that the shared codebook generalizes well across all scenes with a small drop in performance compared to learning a codebook for each scene. Sharing learnt codebook can further reduce the memory requirement and can help speed up the training of CompGS. The quality of the codebook can be improved by learning it over multiple scenes.

5 Conclusion

3D Gaussian Splatting efficiently models 3D radiance fields, outperforming NeRF in learning and rendering efficiency at the cost of increased storage. To reduce storage demands, we apply opacity regularization and K-means-based vector quantization, compressing indices and employing a compact codebook. Our method cuts the storage cost of 3DGs by almost $45\times$, increases rendering FPS by $2.5\times$ while maintaining image quality across benchmarks.

Acknowledgments: This work is partially funded by NSF grant 1845216 and DARPA Contract No. HR00112190135 and HR00112290115.

References

1. Official code repository of 3d gaussian splatting for real-time radiance field rendering. <https://github.com/graphdeco-inria/gaussian-splatting> 7
2. Abbasi Koohpayegani, S., Tejankar, A., Pirsiavash, H.: Compress: Self-supervised learning by compressing representations. Advances in Neural Information Processing Systems **33**, 12980–12992 (2020) 5
3. Ba, L.J., Caruana, R.: Do deep nets really need to be deep? arXiv preprint arXiv:1312.6184 (2013) 5
4. Barron, J.T., Mildenhall, B., Verbin, D., Srinivasan, P.P., Hedman, P.: Mip-nerf 360: Unbounded anti-aliased neural radiance fields. In: Proceedings of the IEEE/CVF Conference on Computer Vision and Pattern Recognition. pp. 5470–5479 (2022) 4, 6, 8, 9

Dataset	Mip-NeRF360	SSIM \uparrow	PSNR \uparrow	LPIPS \downarrow
Method				
3DGs	0.815	27.21	0.214	
3DGs *	0.813	27.42	0.217	
CompGS 4k	0.804	26.97	0.234	
CompGS Shared Codebook	0.797	26.64	0.242	

Fig. 5: Effect of shared codebook.

A frozen codebook trained on one scene (‘Counter’ scene) generalizes well to all other scenes in MipNeRF-360 dataset. Only code assignments are learnt during training.

5. Baruch, G., Chen, Z., Dehghan, A., Dimry, T., Feigin, Y., Fu, P., Gebauer, T., Joffe, B., Kurz, D., Schwartz, A., Shulman, E.: Arkitscenes - a diverse real-world dataset for 3d indoor scene understanding using mobile rgb-d data. In: NeurIPS (2021), <https://arxiv.org/pdf/2111.08897.pdf> 12
6. Baruch, G., Chen, Z., Dehghan, A., Feigin, Y., Fu, P., Gebauer, T., Kurz, D., Dimry, T., Joffe, B., Schwartz, A., Shulman, E.: ARKitscenes: A diverse real-world dataset for 3d indoor scene understanding using mobile RGB-d data. In: Thirty-fifth Conference on Neural Information Processing Systems Datasets and Benchmarks Track (Round 1) (2021), https://openreview.net/forum?id=tjZjv_qh_CE 3, 8
7. Bengio, Y., Léonard, N., Courville, A.: Estimating or propagating gradients through stochastic neurons for conditional computation. arXiv preprint arXiv:1308.3432 (2013) 6
8. Chen, A., Xu, Z., Geiger, A., Yu, J., Su, H.: Tensorf: Tensorial radiance fields. In: European Conference on Computer Vision. pp. 333–350. Springer (2022) 4, 5
9. Chen, G., Choi, W., Yu, X., Han, T., Chandraker, M.: Learning efficient object detection models with knowledge distillation. In: Proceedings of the 31st International Conference on Neural Information Processing Systems. pp. 742–751 (2017) 5
10. Chen, Z., Funkhouser, T., Hedman, P., Tagliasacchi, A.: Mobilenerf: Exploiting the polygon rasterization pipeline for efficient neural field rendering on mobile architectures. In: Proceedings of the IEEE/CVF Conference on Computer Vision and Pattern Recognition. pp. 16569–16578 (2023) 4
11. Cho, M., Vahid, K.A., Fu, Q., Adya, S., Del Mundo, C.C., Rastegari, M., Naik, D., Zatloukal, P.: edkm: An efficient and accurate train-time weight clustering for large language models. arXiv preprint arXiv:2309.00964 (2023) 4
12. Cosman, P.C., Oehler, K.L., Riskin, E.A., Gray, R.M.: Using vector quantization for image processing. Proceedings of the IEEE **81**(9), 1326–1341 (1993) 4
13. Deng, C.L., Tartaglione, E.: Compressing explicit voxel grid representations: fast nerfs become also small. In: Proceedings of the IEEE/CVF Winter Conference on Applications of Computer Vision. pp. 1236–1245 (2023) 5
14. Dettmers, T., Lewis, M., Belkada, Y., Zettlemoyer, L.: Llm. int8 (): 8-bit matrix multiplication for transformers at scale. arXiv preprint arXiv:2208.07339 (2022) 4, 9
15. Equitz, W.H.: A new vector quantization clustering algorithm. IEEE transactions on acoustics, speech, and signal processing **37**(10), 1568–1575 (1989) 4
16. Fan, Z., Wang, K., Wen, K., Zhu, Z., Xu, D., Wang, Z.: Lightgaussian: Unbounded 3d gaussian compression with 15x reduction and 200+ fps. arXiv preprint arXiv:2311.17245 (2023) 5
17. Flynn, J., Neulander, I., Philbin, J., Snavely, N.: Deepstereo: Learning to predict new views from the world’s imagery. In: Proceedings of the IEEE conference on computer vision and pattern recognition. pp. 5515–5524 (2016) 4
18. Fridovich-Keil, S., Yu, A., Tancik, M., Chen, Q., Recht, B., Kanazawa, A.: Plenoxels: Radiance fields without neural networks. In: Proceedings of the IEEE/CVF Conference on Computer Vision and Pattern Recognition. pp. 5501–5510 (2022) 4, 9
19. Garbin, S.J., Kowalski, M., Johnson, M., Shotton, J., Valentin, J.: Fastnerf: High-fidelity neural rendering at 200fps. In: Proceedings of the IEEE/CVF International Conference on Computer Vision. pp. 14346–14355 (2021) 4
20. Gersho, A., Gray, R.M.: Vector quantization and signal compression, vol. 159. Springer Science & Business Media (2012) 4

21. Girish, S., Gupta, K., Shrivastava, A.: Eagles: Efficient accelerated 3d gaussians with lightweight encodings. arXiv preprint arXiv:2312.04564 (2023) [5](#)
22. Gong, Y., Liu, L., Yang, M., Bourdev, L.: Compressing deep convolutional networks using vector quantization. arXiv preprint arXiv:1412.6115 (2014) [4](#)
23. Gray, R.: Vector quantization. *IEEE Assp Magazine* **1**(2), 4–29 (1984) [4](#)
24. Gu, S., Chen, D., Bao, J., Wen, F., Zhang, B., Chen, D., Yuan, L., Guo, B.: Vector quantized diffusion model for text-to-image synthesis. In: Proceedings of the IEEE/CVF Conference on Computer Vision and Pattern Recognition. pp. 10696–10706 (2022) [4](#)
25. Gupta, S., Agrawal, A., Gopalakrishnan, K., Narayanan, P.: Deep learning with limited numerical precision. In: International conference on machine learning. pp. 1737–1746. PMLR (2015) [5](#)
26. Han, S., Mao, H., Dally, W.J.: Deep compression: Compressing deep neural networks with pruning, trained quantization and huffman coding. arXiv preprint arXiv:1510.00149 (2015) [4](#), [5](#)
27. Hedman, P., Philip, J., Price, T., Frahm, J.M., Drettakis, G., Brostow, G.: Deep blending for free-viewpoint image-based rendering. *ACM Transactions on Graphics (ToG)* **37**(6), 1–15 (2018) [4](#), [8](#)
28. Hedman, P., Srinivasan, P.P., Mildenhall, B., Barron, J.T., Debevec, P.: Baking neural radiance fields for real-time view synthesis. In: Proceedings of the IEEE/CVF International Conference on Computer Vision. pp. 5875–5884 (2021) [4](#)
29. Henzler, P., Mitra, N.J., Ritschel, T.: Escaping plato’s cave: 3d shape from adversarial rendering. In: Proceedings of the IEEE/CVF International Conference on Computer Vision. pp. 9984–9993 (2019) [4](#)
30. Hinton, G., Vinyals, O., Dean, J.: Distilling the knowledge in a neural network. arXiv preprint arXiv:1503.02531 (2015) [5](#)
31. Huang, B., Yan, X., Chen, A., Gao, S., Yu, J.: Pref: Phasorial embedding fields for compact neural representations. arXiv preprint arXiv:2205.13524 (2022) [5](#)
32. Jacob, B., Kligys, S., Chen, B., Zhu, M., Tang, M., Howard, A., Adam, H., Kalenichenko, D.: Quantization and training of neural networks for efficient integer-arithmetic-only inference. In: Proceedings of the IEEE Conference on Computer Vision and Pattern Recognition. pp. 2704–2713 (2018) [4](#), [5](#)
33. Kerbl, B., Kopanas, G., Leimkühler, T., Drettakis, G.: 3d gaussian splatting for real-time radiance field rendering. *ACM Transactions on Graphics (ToG)* **42**(4), 1–14 (2023) [1](#), [3](#), [4](#), [5](#), [7](#), [8](#), [9](#), [20](#)
34. Knapitsch, A., Park, J., Zhou, Q.Y., Koltun, V.: Tanks and temples: Benchmarking large-scale scene reconstruction. *ACM Transactions on Graphics (ToG)* **36**(4), 1–13 (2017) [8](#)
35. Krishnamoorthi, R.: Quantizing deep convolutional networks for efficient inference: A whitepaper. arXiv preprint arXiv:1806.08342 (2018) [4](#), [5](#)
36. Lee, J.C., Rho, D., Sun, X., Ko, J.H., Park, E.: Compact 3d gaussian representation for radiance field. arXiv preprint arXiv:2311.13681 (2023) [5](#)
37. Lee, Y.Y., Woods, J.W.: Motion vector quantization for video coding. *IEEE Transactions on Image Processing* **4**(3), 378–382 (1995) [4](#)
38. Li, L., Shen, Z., Wang, Z., Shen, L., Bo, L.: Compressing volumetric radiance fields to 1 mb. In: Proceedings of the IEEE/CVF Conference on Computer Vision and Pattern Recognition. pp. 4222–4231 (2023) [5](#)
39. Li, L., Shen, Z., Wang, Z., Shen, L., Tan, P.: Streaming radiance fields for 3d video synthesis. *Advances in Neural Information Processing Systems* **35**, 13485–13498 (2022) [5](#)

40. Makhoul, J., Roucos, S., Gish, H.: Vector quantization in speech coding. *Proceedings of the IEEE* **73**(11), 1551–1588 (1985) [4](#)
41. Mildenhall, B., Srinivasan, P.P., Tancik, M., Barron, J.T., Ramamoorthi, R., Ng, R.: Nerf: Representing scenes as neural radiance fields for view synthesis. In: *Proceedings of the European Conference on Computer Vision (ECCV)* (2020), <http://arxiv.org/abs/2003.08934v2> [1](#), [4](#), [20](#)
42. Morgenstern, W., Barthel, F., Hilsmann, A., Eisert, P.: Compact 3d scene representation via self-organizing gaussian grids. *arXiv preprint arXiv:2312.13299* (2023) [5](#)
43. Müller, T., Evans, A., Schied, C., Keller, A.: Instant neural graphics primitives with a multiresolution hash encoding. *ACM Transactions on Graphics (ToG)* **41**(4), 1–15 (2022) [4](#), [5](#), [9](#)
44. Niedermayr, S., Stumpfegger, J., Westermann, R.: Compressed 3d gaussian splatting for accelerated novel view synthesis. *arXiv preprint arXiv:2401.02436* (2023) [5](#)
45. Nooralinejad, P., Abbasi, A., Koohpayegani, S.A., Meibodi, K.P., Khan, R.M.S., Kolouri, S., Pirsavash, H.: Pranc: Pseudo random networks for compacting deep models. In: *Proceedings of the IEEE/CVF International Conference on Computer Vision*. pp. 17021–17031 (2023) [5](#)
46. Peng, S., Jiang, C., Liao, Y., Niemeyer, M., Pollefeys, M., Geiger, A.: Shape as points: A differentiable poisson solver. *Advances in Neural Information Processing Systems* **34**, 13032–13044 (2021) [4](#)
47. Penner, E., Zhang, L.: Soft 3d reconstruction for view synthesis. *ACM Transactions on Graphics (TOG)* **36**(6), 1–11 (2017) [4](#)
48. Polino, A., Pascanu, R., Alistarh, D.: Model compression via distillation and quantization. *arXiv preprint arXiv:1802.05668* (2018) [5](#)
49. Rastegari, M., Ordonez, V., Redmon, J., Farhadi, A.: Xnor-net: Imagenet classification using binary convolutional neural networks (2016) [2](#)
50. Rastegari, M., Ordonez, V., Redmon, J., Farhadi, A.: Xnor-net: Imagenet classification using binary convolutional neural networks. In: Leibe, B., Matas, J., Sebe, N., Welling, M. (eds.) *Computer Vision - ECCV 2016 - 14th European Conference, Amsterdam, The Netherlands, October 11–14, 2016, Proceedings, Part IV. Lecture Notes in Computer Science*, vol. 9908, pp. 525–542. Springer (2016). https://doi.org/10.1007/978-3-319-46493-0_32, https://doi.org/10.1007/978-3-319-46493-0_32 [4](#)
51. Razavi, A., Van den Oord, A., Vinyals, O.: Generating diverse high-fidelity images with vq-vae-2. *Advances in neural information processing systems* **32** (2019) [4](#)
52. Reiser, C., Peng, S., Liao, Y., Geiger, A.: Kilonerf: Speeding up neural radiance fields with thousands of tiny mlps. In: *Proceedings of the IEEE/CVF International Conference on Computer Vision*. pp. 14335–14345 (2021) [4](#)
53. Riegler, G., Koltun, V.: Free view synthesis. In: *Computer Vision–ECCV 2020: 16th European Conference, Glasgow, UK, August 23–28, 2020, Proceedings, Part XIX 16*. pp. 623–640. Springer (2020) [4](#)
54. Schwarz, K., Sauer, A., Niemeyer, M., Liao, Y., Geiger, A.: Voxgraf: Fast 3d-aware image synthesis with sparse voxel grids. *Advances in Neural Information Processing Systems* **35**, 33999–34011 (2022) [4](#)
55. Sitzmann, V., Thies, J., Heide, F., Nießner, M., Wetzstein, G., Zollhofer, M.: Deepvoxels: Learning persistent 3d feature embeddings. In: *Proceedings of the IEEE/CVF Conference on Computer Vision and Pattern Recognition*. pp. 2437–2446 (2019) [4](#)

56. Sun, C., Sun, M., Chen, H.T.: Direct voxel grid optimization: Super-fast convergence for radiance fields reconstruction. In: Proceedings of the IEEE/CVF Conference on Computer Vision and Pattern Recognition. pp. 5459–5469 (2022) [4](#)
57. Takikawa, T., Evans, A., Tremblay, J., Müller, T., McGuire, M., Jacobson, A., Fidler, S.: Variable bitrate neural fields. In: ACM SIGGRAPH 2022 Conference Proceedings. pp. 1–9 (2022) [4, 5](#)
58. Tang, J., Chen, X., Wang, J., Zeng, G.: Compressible-composable nerf via rank-residual decomposition. In: Advances in Neural Information Processing Systems (2022) [5](#)
59. Thies, J., Zollhöfer, M., Nießner, M.: Deferred neural rendering: Image synthesis using neural textures. *Acm Transactions on Graphics (TOG)* **38**(4), 1–12 (2019) [4](#)
60. Van Den Oord, A., Vinyals, O., et al.: Neural discrete representation learning. *Advances in neural information processing systems* **30** (2017) [4](#)
61. Vanhoucke, V., Senior, A., Mao, M.Z.: Improving the speed of neural networks on cpus (2011) [5](#)
62. Wang, L., Zhang, J., Liu, X., Zhao, F., Zhang, Y., Zhang, Y., Wu, M., Yu, J., Xu, L.: Fourier plenoctrees for dynamic radiance field rendering in real-time. In: Proceedings of the IEEE/CVF Conference on Computer Vision and Pattern Recognition. pp. 13524–13534 (2022) [4](#)
63. Wen, W., Wu, C., Wang, Y., Chen, Y., Li, H.: Learning structured sparsity in deep neural networks. *arXiv preprint arXiv:1608.03665* (2016) [5](#)
64. Wu, X., Xu, J., Zhu, Z., Bao, H., Huang, Q., Tompkin, J., Xu, W.: Scalable neural indoor scene rendering. *ACM Transactions on Graphics (TOG)* (2022) [4](#)
65. Xu, Q., Xu, Z., Philip, J., Bi, S., Shu, Z., Sunkavalli, K., Neumann, U.: Point-nerf: Point-based neural radiance fields. In: Proceedings of the IEEE/CVF Conference on Computer Vision and Pattern Recognition. pp. 5438–5448 (2022) [4](#)
66. Yu, A., Li, R., Tancik, M., Li, H., Ng, R., Kanazawa, A.: Plenoctrees for real-time rendering of neural radiance fields. In: Proceedings of the IEEE/CVF International Conference on Computer Vision. pp. 5752–5761 (2021) [4, 5](#)
67. Zhou, T., Tulsiani, S., Sun, W., Malik, J., Efros, A.A.: View synthesis by appearance flow. In: Computer Vision–ECCV 2016: 14th European Conference, Amsterdam, The Netherlands, October 11–14, 2016, Proceedings, Part IV 14. pp. 286–301. Springer (2016) [4](#)

Appendix

Here, we compare the performance of our CompGS with state-of-the-art approaches on the NeRF-Synthetic dataset (Section A). Section B shows exploratory results on generalization of the learnt vector codebook across scenes and Section C provides insights on the learnt codebook assignments. We also provide scene-wise results (section D), ablations on baselines (section E) and additional visualizations and qualitative comparisons on the ARKit dataset (section F).

A Results on NeRF-Synthetic dataset

The results (PSNR) for the NeRF-Synthetic dataset [41] are presented in Table A.1. Our CompGS approach achieves an impressive average improvement of 1.13 points in PSNR compared to the 3DGS-No-SH baseline while using less than half its memory. As reported in the main submission, we report metrics for 3DGS both from the original paper and using our own runs. We observe an improvement for 3DGS [33] over their official reported numbers by 0.5 points.

Table A.1: Results on NeRF-Synthetic dataset. Here, we present the PSNR values for the synthesized novel views on the NeRF-Synthetic dataset [41]. Our CompGS approach achieves an impressive average improvement of 1.13 points in PSNR compared to the 3DGS-No-SH baseline while using less than half its memory. As reported in the main submission, we report metrics for 3DGS both from the original paper and using our own runs. We observe an improvement of 3DGS over the reported numbers by 0.5points. * indicates our own run.

	Mic	Chair	Ship	Materials	Lego	Drums	Ficus	Hotdog	Avg.
Plenoxels	33.26	33.98	29.62	29.14	34.10	25.35	31.83	36.81	31.76
INGP-Base	36.22	35.00	31.10	29.78	36.39	26.02	33.51	37.40	33.18
Mip-Nerf	36.51	35.14	30.41	30.71	35.70	25.48	33.29	37.48	33.09
Point-NeRF	35.95	35.40	30.97	29.61	35.04	26.06	36.13	37.30	33.30
3DGS	35.36	35.83	30.80	30.00	35.78	26.15	34.87	37.72	33.32
3DGS*	36.80	35.51	31.69	30.48	36.06	26.28	35.49	38.06	33.80
3DGS-No-SH	34.37	34.09	29.86	28.42	34.84	25.48	32.30	36.43	31.97
CompGS 4k	35.99	34.92	31.05	29.74	35.09	25.93	35.04	37.04	33.10

B Generalization of codebook across scenes

We train our vector quantization approach including the codebook and the code assignments on a single scene ('Counter') of the Mip-NeRF360 dataset. We then

freeze the codebook and learn only assignments for the rest of the eight scenes in the dataset and report the averaged performance metrics over all scenes. In addition to the results in Fig.5 of the main submission, we provide results with our 32K variant here in table B.2. Interestingly, we observe that the shared codebook generalizes well across all scenes with a small drop in performance compared to learning a codebook for each scene. Sharing learnt codebook can further reduce the memory requirement and can help speed up the training of CompGS. The quality of the codebook can be improved by learning it over multiple scenes. Fig. F.3 shows qualitative comparison of the same. There are no apparent differences between CompGS and CompGS-Shared-Codebook approaches.

Table B.2: Effect of shared codebook. We train our vector quantization approach including the codebook and the code assignments on a single scene (‘Counter’) of the Mip-NeRF360 dataset. We then freeze the codebook and learn only assignments for the rest of the eight scenes in the dataset and report the averaged performance metrics over all scenes. Interestingly, we observe that the shared codebook generalizes well across all scenes with a small drop in performance compared to learning a codebook for each scene. Sharing learnt codebook can further reduce the memory requirement and can help speed up the training of CompGS. The quality of the codebook can be improved by learning it over multiple scenes.

Dataset Method	Mip-NeRF360		
	SSIM $^{\uparrow}$	PSNR $^{\uparrow}$	LPIPS $^{\downarrow}$
3DGS	0.815	27.21	0.214
3DGS *	0.813	27.42	0.217
CompGS 4K	0.804	26.97	0.234
CompGS 32K	0.806	27.12	0.240
CompGS Shared Codebook 4K	0.797	26.64	0.242
CompGS Shared Codebook 32K	0.800	26.780	0.247

C Analysis of learnt code assignments

In Fig. C.1, we plot the sorted histogram of the code assignments (cluster to which each Gaussian belongs to) for each parameter on the ‘Train’ scene of Tanks&Temples dataset. We observe that just a single code out of the 512 in total is assigned to nearly 5% of the Gaussians for both the SH and DC parameters. Similarly, a few clusters dominate even in the case of rotation and scale parameters, albeit to a lower extent. Such a non-uniform distribution of cluster sizes suggest that further compression can be achieved by using Huffman coding to store the assignment indices.

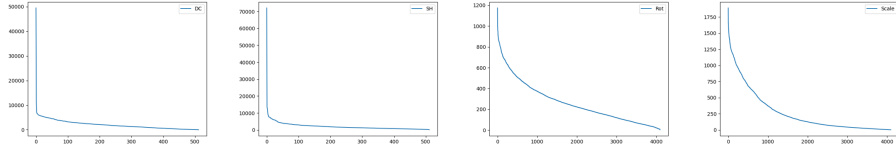


Fig. C.1: Histogram of code assignments. We plot the sorted histogram of the code assignments (cluster to which each Gaussian belongs to) for each parameter on the ‘Train’ scene of Tanks&Temples dataset. We observe that just a single code out of the 512 in total is assigned to nearly 5% of the Gaussians for both the SH and DC parameters. Similarly, a few clusters dominate even in the case of rotation and scale parameters, albeit to a lower extent. Such a non-uniform distribution of cluster sizes suggest that further compression can be achieved by using Huffman coding to store the assignment indices.

D Scene-wise Metrics

For brevity, we reported the averaged metrics over all scenes in a dataset in our main submission. Here in table D.3, we provide the detailed scene-wise metrics for MipNerf-360, Tanks and Temples and DeepBlending datasets.

E Ablations for Gaussian count reduction

We perform ablations to choose the right hyperparameters for the baseline approaches to reduce the Gaussian count. The metrics for the chosen settings are reported in table 3 of the main submission. The ablations for minimum opacity, densification interval and end iteration and gradient threshold are shown in tables E.4, E.5, E.6 and E.7 respectively. Among these baselines, modify gradient threshold provides the best trade-off between model size and performance.

F Qualitative comparison on ARKit dataset.

Figures F.4 and F.5 provide qualitative results on the ARKit dataset.

Table D.3: Scene-wise metrics. We report the scene-wise metrics on all the scenes for both 3DGS and CompGS 32K. As observed in the averaged metrics in the main submission, CompGS achieves a high level of compression and fast rendering without losing much on rendering quality.

Scene	Method	SSIM $^{\uparrow}$	PSNR $^{\uparrow}$	LPIPS $^{\downarrow}$	Train Time(s)	FPS	Mem(MB)	#Gauss
Bicycle	3DGS	0.763	25.169	0.212	1845	68	1422	6026079
	CompGS 32K	0.755	25.068	0.244	2123	242	29	1314018
Bonsai	3DGS	0.940	31.918	0.206	876	276	293	1241520
	CompGS 32K	0.932	31.195	0.223	1405	492	10	377227
Counter	3DGS	0.906	29.018	0.202	968	208	283	1200091
	CompGS 32K	0.895	28.467	0.222	1571	356	10	385515
Flowers	3DGS	0.602	21.456	0.339	1192	133	851	3605827
	CompGS 32K	0.588	21.262	0.367	1744	343	23	1037132
Garden	3DGS	0.863	27.241	0.108	1870	76	1347	5709543
	CompGS 32K	0.848	26.822	0.140	2177	258	30	1370624
Kitchen	3DGS	0.926	31.510	0.127	1206	158	425	1801403
	CompGS 32K	0.918	30.774	0.142	1729	317	13	564382
Room	3DGS	0.917	31.346	0.221	1020	190	364	1541909
	CompGS 32K	0.912	31.131	0.235	1439	444	9	327191
Stump	3DGS	0.772	26.651	0.215	1445	104	1136	4815087
	CompGS 32K	0.770	26.605	0.236	1936	303	27	1226044
Treehill	3DGS	0.633	22.504	0.327	1213	122	879	3723675
	CompGS 32K	0.634	22.747	0.355	1744	336	23	1002290
Train	3DGS	0.811	21.991	0.209	563	253	254	1077461
	CompGS 32K	0.804	21.789	0.231	1169	456	12	500811
Truck	3DGS	0.878	25.385	0.148	897	159	611	2588966
	CompGS 32K	0.872	25.092	0.165	1306	494	13	540081
DrJohnson	3DGS	0.898	29.089	0.247	1312	121	772	3270679
	CompGS 32K	0.906	29.445	0.249	1717	379	17	714902
Playroom	3DGS	0.901	29.903	0.246	1003	181	551	2335846
	CompGS 32K	0.908	30.347	0.253	1422	589	10	393414

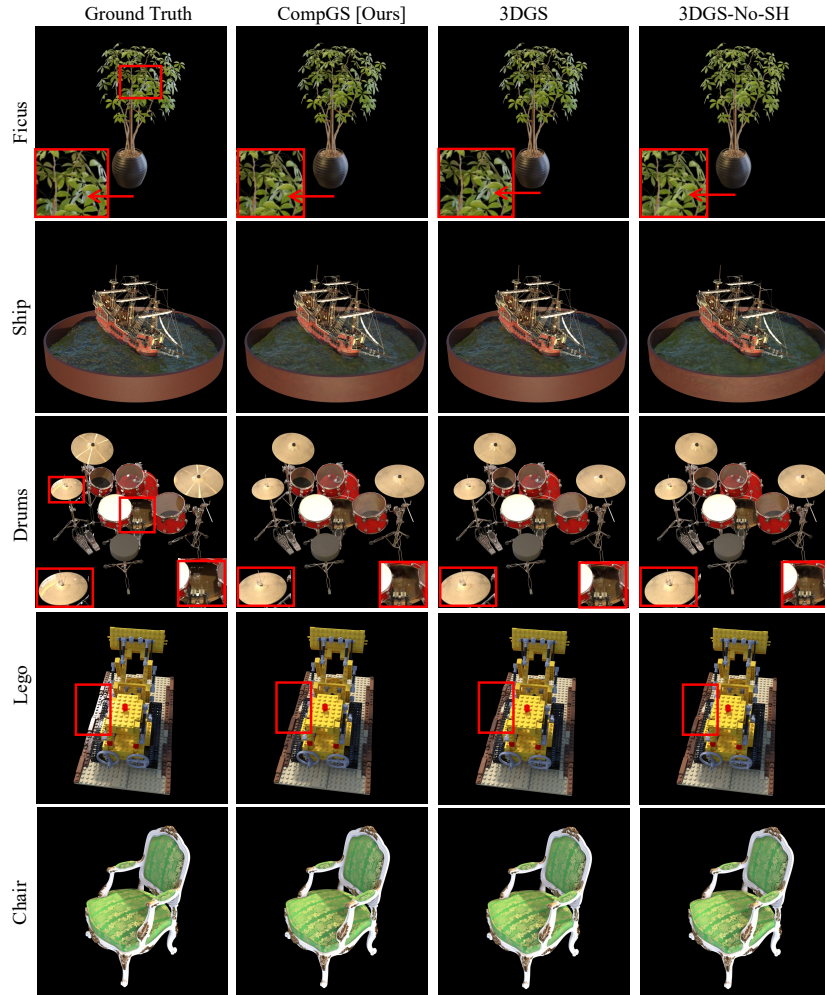


Fig. F.2: Visualization of results on Sythentic-NeRF dataset. We compare the performance of our compressed CompGS with the original 3DGS and 3DGS-No-SH approaches on different scenes of the NeRF-Synthetic dataset. The difference between CompGS and 3DGS-No-SH is apparent in some of these scenes. E.g., 3DGS-No-SH fails to effectively model the brown color of branches and shadows and bright light on the leaves of the ‘Ficus’ scene. All approaches including 3DGS have imperfect reconstruction in some of the scenes like ‘Drums’ and ‘Lego’. The scenes and views used for visualization were chosen at random.

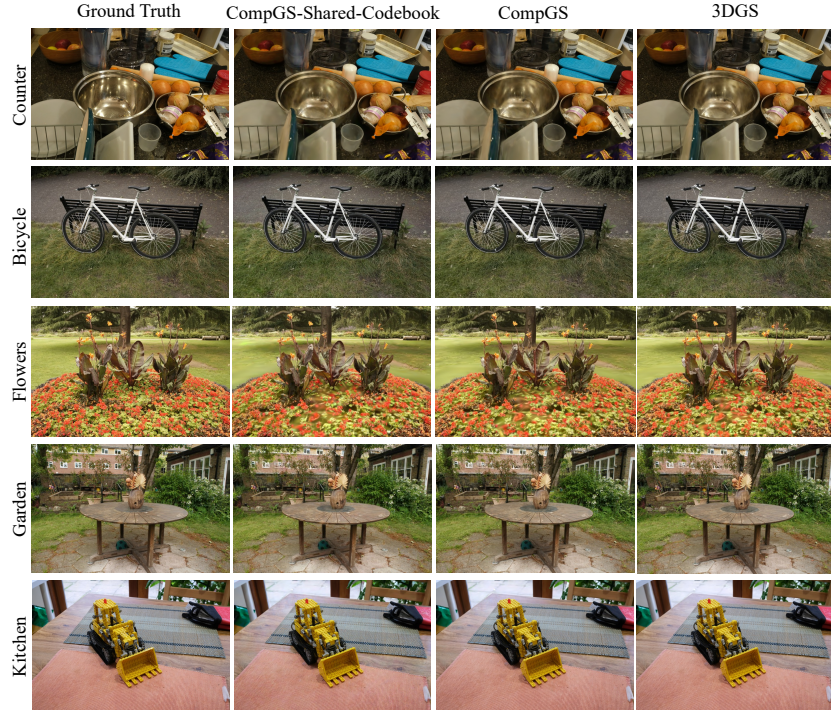


Fig. F.3: Qualitative analysis of shared codebook. We show the generalization of codebook learned using a single scene on various scenes of the Mip-NeRF360 dataset. The codebook was trained on the ‘Counter’ scene (row-1) and frozen for the remaining scenes. The codebooks for all four parameters (DC, SH, Scale, Rot) are shared across scenes. Both CompGS and CompGS-Shared-Codebook are visually similar to the uncompressed 3DGS with no conspicuous differences between them. 3DGS-No-SH requires twice more memory than CompGS while 3DGS is ten times bigger than CompGS . The scenes and views used for visualization were chosen at random.

Table E.4: Ablation study on opacity threshold. We changed the default value of 0.005 for minimum opacity as a baseline approach for compressing 3DGS by reducing the number of Gaussians. Gaussians with opacity values below the threshold are pruned, resulting in smaller models for lower thresholds. Table 3 in main paper shows the results of this experiment when min opacity is 0.1.

	Mip-NeRF360				Tanks&Temples				Deep Blending			
	SSIM	PSNR	LPIPS	#Gauss	SSIM	PSNR	LPIPS	#Gauss	SSIM	PSNR	LPIPS	#Gauss
0.05	0.810	27.308	0.230	1.93M	0.839	23.508	0.194	1.04M	0.902	29.542	0.251	1.47M
0.1	0.802	27.120	0.244	1.46M	0.833	23.439	0.204	780K	0.902	29.504	0.255	1.01M

Table E.5: Ablation study on densification interval. We modify the densification interval in 3DGS as a baseline approach for compressing 3DGS by reducing the number of Gaussians. Higher intervals results in less frequent densification and thus smaller number of Gaussians. Table 3 in main paper shows the results of this experiment when interval is 500.

	Mip-NeRF360				Tanks&Temples				Deep Blending			
	SSIM	PSNR	LPIPS	#Gauss	SSIM	PSNR	LPIPS	#Gauss	SSIM	PSNR	LPIPS	#Gauss
300	0.803	27.201	0.241	1.70M	0.837	23.517	0.195	1.00M	0.902	29.705	0.253	1.30M
500	0.794	26.98	0.255	1.07M	0.832	23.36	0.206	709K	0.902	29.76	0.258	844K

Table E.6: Ablation study on densification end iteration. Early or late stopping of densification process impacts the number of Gaussians and the model performance of 3DGS. We report the results with the value set to 3000 in our main submission (table 3).

	Mip-NeRF360				Tanks&Temples				Deep Blending			
	SSIM	PSNR	LPIPS	#Gauss	SSIM	PSNR	LPIPS	#Gauss	SSIM	PSNR	LPIPS	#Gauss
5000	0.797	27.199	0.241	1.92M	0.838	23.599	0.188	1.12M	0.897	29.486	0.256	1.34M
3000	0.780	27.02	0.267	1.12M	0.835	23.55	0.194	810K	0.896	29.42	0.264	795K

Table E.7: Ablation study on gradient threshold. We modify the gradient threshold, used as a criterion in the densification process of 3DGS. A higher threshold results in a smaller 3DGS model. Among the baselines considered for reducing Gaussian count, modify gradient threshold provides the best trade-off between model size and performance. Table 3 in main paper shows the results of this experiment for gradient threshold of 0.00045.

	Mip-NeRF360				Tanks&Temples				Deep Blending			
	SSIM	PSNR	LPIPS	#Gauss	SSIM	PSNR	LPIPS	#Gauss	SSIM	PSNR	LPIPS	#Gauss
0.00035	0.786	26.934	0.265	1.27M	0.833	23.579	0.203	833K	0.901	29.574	0.254	1.41M
0.00045	0.769	26.57	0.292	809K	0.825	23.31	0.217	578K	0.900	29.49	0.260	1.01M
0.00055	0.754	26.290	0.312	552K	0.818	23.041	0.228	433K	0.899	29.544	0.265	764K



Fig. F.4: Visualization of ARKit dataset. ARKit is a 3D indoor scene dataset captured using a iPads/iPhones. The dataset consists of videos of indoor environments like houses and office space from multiple view-points. We uniform sample images from each video to form our benchmark dataset for novel view synthesis. Some sample images from different scenes are shown in this figure. The dataset presents unique challenges such as the presence of motion blur due to the use of videos.



Fig. F.5: Qualitative analysis on ARKit dataset. We visualize the results of CompGS along with the uncompresssed 3DGS and its variant 3DGS-No-SH. Presence of large noisy blobs is a common error mode for 3DGS-No-SH on this dataset. It also fails to faithfully reproduce the colors and lighting in several scenes. The visual quality of the synthesized images for all methods is lower on this dataset compared to the scenes present in standard benchmarks like Mip-NeRF360, indicating its utility as a novel benchmark. Further comparison with various NeRF based approaches and more analysis can help improve the results on this dataset.